Geotech Geol Eng (2022) 40:1739–1750
https://doi.org/10.1007/s10706-021-01990-x

ORIGINAL PAPER

Experimental study on impact signal frequency spectrum and energy distribution characteristics of water-stone flow

Xuehai Liao · Hongkai Chen · Jinhao Zhang · Kai Su

Received: 5 July 2021 / Accepted: 5 September 2021 / Published online: 17 September 2021

Abstract Understanding of impact characteristics is the basis of studying the hydrodynamic characteristics of water–rock flow. The impact and vibration characteristics of water-stone flow on protective structures were comprehensively studied in the research presented in this paper using an indoor large-scale test. Five groups (A–E) of graded crushed stone particles, combined with six levels of solid–liquid ratio (0.01, 0.05, 0.10, 0.15, 0.20, and 0.25) were used in this testing program. The spectrum and the energy spectrum of impact acceleration signal were analyzed and pertinent information was extracted using wavelet theory. The test results showed that the auto correlation curve of the impact signal had a maximum value when the delay of impact acceleration signal (τ) was zero, and the curves on both sides of the instant of impact were non-periodic, indicating that the periodicity of the signal was poor. However, two observed impulse signals were stable and they highly correlated. Maximum energy of the shock signal was located in the low frequency within an approximate coefficient a_8 band, and the maximum amplitude of each band decayed from a low frequency (a_8: 0–0.3905 Hz) to an high frequency (d_5: 3.125–6.25 Hz), while the attenuation amplitude decreased gradually. The real impact acceleration signal of the water-stone flow was in the band of 0–6.25 Hz, and the rest were a result of signal noise. The research provided a new and innovative methodology of studying the impact characteristics of such debris flow, and also provided some significant guidance for the design of water-stone flow disaster prevention structures.

Keywords Water-stone flow · Model test · Impact signal frequency spectrum · Energy distribution characteristics · Disaster prevention and control

X. Liao (✉)
Institue of Geotechnical Engineering, Chongqing Jiaotong University, Chongqing 400071, China
e-mail: cqjtulxh@163.com

X. Liao
Nanjiang Hydrogeological and Engineering Geology Brigade, Chongqing Institute of Geology and Mineral Resources Survey, Chongqing 401147, China

H. Chen · J. Zhang
School of City and Architecture Engineering, Zaozhuang University, Zaozhuang 277160, Shandong, China

K. Su
China Construction Seventh Engineering Division. Corp. Ltd, Zhengzhou 450000, Henan, China

1 Introduction

Water-stone flow has common characteristics such as suddenness, extensiveness, and a usually strong catastrophic event. It is affected by solid particles and their movement characteristics, such as small bulk density, low viscosity, and strong collision events

between particles (Wang et al. 2020; Zhang 2009). Water-stone flow will cause serious harm to other structures such as highways, tunnels, environment and flood drainage flumes (Yang et al. 2014; Wu et al. 2021). China has many debris flow flumes, with developed monitoring, early warning, and comprehensive treatment technologies, but the basic underlying theoretical research on debris flow still needs to be strengthened (Cui 2009). The characteristics of the impact acceleration signal in the frequency domain can be described by analyzing the power spectrum function of the impact acceleration signal of the water-stone flow. These being the spectral characteristics and signal density characteristics of the impact acceleration signal, so as to further reflectively define the movement characteristics of the water-stone flow.

Due to the suddenness and the potential disaster characteristics of water-stone flows, the impact characteristics of water-stone flows were mainly studied through indoor models or tank tests. For example, Xu et al. (2000) used the water trough to simulate the water–rock flow segmented with characteristics of coarse solid particles and low clay content, to solve the discontinuous similarity of the solid-phase particle gradation through the methods of geometric rate and variable particle size scale. Savage (1979) revealed the motion characteristics as being non-viscous particle flow through the water tank experiment, and analyzed the dynamic effects of particle flow; side wall friction, faucet jumping and particle bounce. Nearing et al. (1999) and Strutinskiy et al. (2018) studied the entrainment effects of water flow on specific rocks and surface sediment, and deduced relationships between the flow velocity, flow rate and the properties of solid particles entrained by the scour. They further pointed out that on a rough surface, the flood velocity was related to the flow and hydraulic radius, but not to the slope. Guo et al. (2014) used a two-phase fluid model to calculate the stable flow velocity of debris flow along the riverbed and the role of solid and liquid phases on the impact characteristics of debris flow. Ma et al. (2016) and Chen et al. (2016) studied the flow control and Catastrophe Characteristics of water-stone flow start, and obtained the relationship between the thickness of water-stone movement and the required flow when water-stone start and the relationship between the density of water-stone. He et al. (2014) used the debris flow impact test model and found that the average impact load of the water-stone flow was proportional to the solid–liquid ratio and the particle size: larger the solid-to-liquid ratio, smaller was the impact of the water-stone flow faucet, whereas with larger particle size greater was the impact on load changes. Chechelnitsky et al. (2018) reported on the results of the seismic studied on the disastrous water-stone flow passing down the Kyngarga River. The paper showed that the period of the flow activity of debris was accompanied by a change in the properties of microseisms, including the high-frequency component (22–48 Hz) associated with the motion of the solid fraction and the low-frequency component (0.35–0.45 Hz) associated with the water displacement.

There were moving average method (Hu et al. 2011) and wavelet de-noising method (Wang et al. 2020; Tang et al. 2013) used in the water-stone flow shock acceleration signal processing. The analysis method of ground motion can also be used for reference (Zhuang et al. 2015; Ding et al. 2019). However, the wavelet method was the main and popular method. For example, Zhang et al (2019) pointed out that the measured signal from the acceleration sensor contained noise interference, and analyzed the wavelet hard threshold and soft threshold denoising methods with their respective advantages and disadvantages. Wang et al (2019) used wavelet theory to analyze the dynamic characteristics of the impact acceleration signal of the energy dissipation shed. He et al. (2016) used the wavelet method to analyze and extract the energy distribution characteristics from the impact acceleration signal of the debris flow.

In order to explore the impact and vibration characteristics of water rock flow on bridge pier and other structures, water-stone flow impact model tests with different solid–liquid ratios were carried out in this research with different particle grading, in order to collect the impact and vibration characteristics of water-stone flow on a structure. The wavelet method was used to process the impact acceleration signal and analyze the signal's frequency spectrum and energy distribution characteristics, defining the characteristics of the water-stone flow and signal distribution for the indoor model test conditions. The research output and methodology have positive contributions to the expansion of debris flow research and testing methods to help disaster prevention and mitigation.

2 Experimental model and working condition design

2.1 Experimental model design

The debris flow in Qipangou, Sichuan Province was used as a prototype to build an experimental model of the impact of the debris flow in the valley. Apart from considering similar dimensions, the model included: model experiment platform, water and stone supply system and impact acceleration test system, etc. (Fig. 1). The debris flow flume was U-shaped, with an oblique length of 1060 cm, a height difference of 305 cm, a slope of 10°–36°, and a low roughness. The net water storage capacity in the water supply tank was 1.04 m^3, and the source tank could store about 600 kg of graded gravel. The bottom of the water tank and the bottom of the source tank were inter-connected with a 30 cm diameter pipe. The water output and the feeding speed of graded crushed stone particles were controlled via automatic control valves. Incorporating a DH5922D dynamic signal test system, the impact vibration acceleration signal of the water-stone flow was collected by installing the Donghua 1A702E underwater uniaxial piezoelectric acceleration sensor (Fig. 2) in the flume. The overall size of the sensor (length × width × height) is 27.5 × 26.5 × 20 mm, with an axial sensitivity of 0 ∼ 10 mV/m s^{-2} and a frequency response of 0.5–10000 Hz, and the amplitude is − 918 to 918 m s^{-2}.

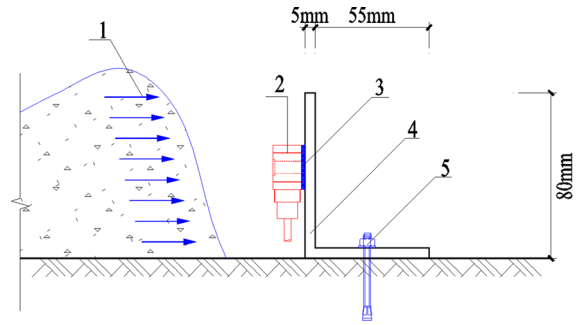

Fig. 2 Sensor installation diagram. 1-Water–rock flow; 2-Vibration acceleration sensor; 3-Modified acrylic adhesive; 4-Steel plate; 5-Expansion bolt

2.2 Experimental condition design and data acquisition

The experiment, which was an indoor water-stone flow model experiment, used an impact acceleration sensor to monitor the impact motion characteristics of the water-stone flow (under a known condition of solid–liquid ratio) and a specific grade of granular crushed stone particles. The experiment material comprised of 5 groups of particle-graded solid phases A–E (0–5 mm, 5–10 mm, 10–15 mm, 15–20 mm and 20–25 mm) prepared with sieved single sized crushed stone particles, as shown in Fig. 3. The composition of graded crushed stone, its uneven coefficient C_u and its curvature coefficient C_c are shown in Table 1.

According to the appropriate particle grading group and the 6 levels of solid–liquid ratios (ratio of solid mass to liquid mass) of 0.01, 0.05, 0.10, 0.15, 0.20 and 0.25 set in the test, the test graded gravel materials

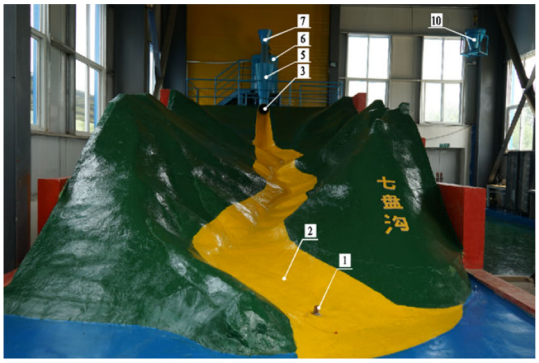

(a) Model test platform

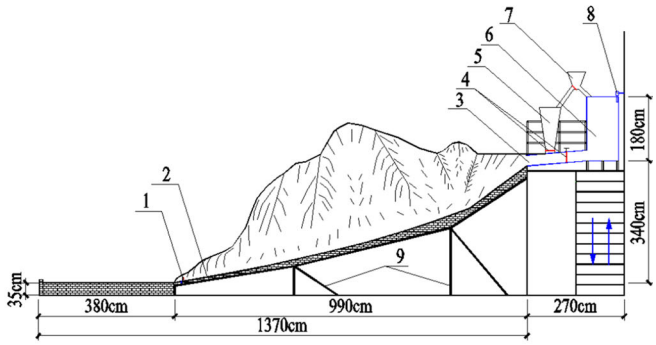

(b) Model test platform profile

Fig. 1 Experimental model of water-stone flow. 1-Vibration acceleration sensor; 2-Debris flow flume; 3-Water outlet; 4-Gate; 5-Stone; 6-Water; 7-Diverter valve; 8-Water intake; 9-Steel support; 10-Lifting equipment

(a) A: 0–5 mm

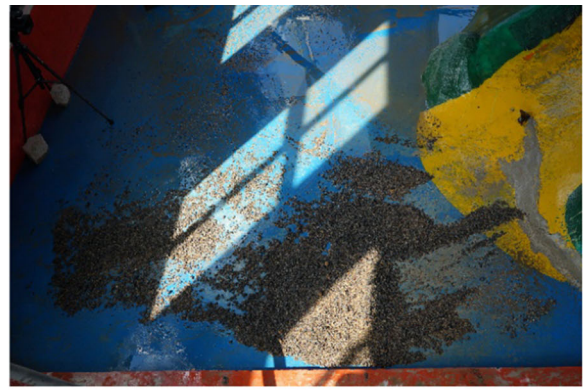

(b) B: 5–10 mm

(c) C: 10–15 mm

(d) D: 15–20 mm

(e) E: 20–25 mm

Fig. 3 Gravel with different particle sizes

were prepared and weighed. Particle grading (5 groups, number A–E) and solid–liquid ratio (6 levels, number 1–6) were combined to constitute 30 test groups. With an additional clean water test, the total number of test conditions was 31. Therefore, as an example of the test nomenclature, C4 represented the combination of group C grading with a solid–liquid ratio of 0.15. As regards to the model debugging

Table 1 Basic grading curve data of the crushed stone particle groups

Groups	Accumulated percentage of particles smaller than size (%)					Non uniform coefficient C_u	Coefficient of curvature C_c
	≤ 5 mm	5–10 mm	10–15 mm	15–20 mm	20–25 mm		
A	80	90	95	98	100	5.61	1.40
B	30	70	90	96	100	5.25	1.82
C	10	30	70	90	100	2.71	1.48
D	4	12	30	70	100	2.05	1.33
E	1	3	7	20	100	1.38	1.14

situation, the effective time of test impact was set at about 60 s, and the sampling frequency was 200 Hz. A total of 39 sets of water-stone flow impact acceleration test data (including 8 sets of repeated tests for individual working conditions) were obtained during this investigation. At the same time, the image data from each test group were recorded using a high-speed camera and the information was used to analyze the movement characteristics of the water-stone flow.

3 Basic processing of impact acceleration signal

3.1 Basic experimental data

The impact of water-stone flow was closely related to its density and velocity, and the basic information of water-stone flow density and velocity was statistically analyzed. In accordance with the experimental conditions, the theoretical density of water-stone flow in each test group was calculated by using Eq. (1).

$$\rho = \frac{m_s + m_l}{V_s + V_l} = \frac{m_s + m_l}{V_s/\rho_s + V_l/\rho_l} \quad (1)$$

where ρ is water-stone flow density (kg/m^3); ρ_s is debris flow density (kg/m^3); ρ_l is water density (kg/m^3); m_s is mass of graded crushed stone (kg); m_l is mass of water (kg); V_s is volume of graded crushed stone (kg); V_l is volume of water (kg).

In each working condition, three groups of water-stone flow samples were collected with a measuring cup at the gully, and then the collected samples were averaged to obtain their density under test conditions, as shown in Fig. 4. The theoretical density and the measured density were compared as shown in Fig. 5.

Fig. 4 Water-stone flow density test under different working conditions

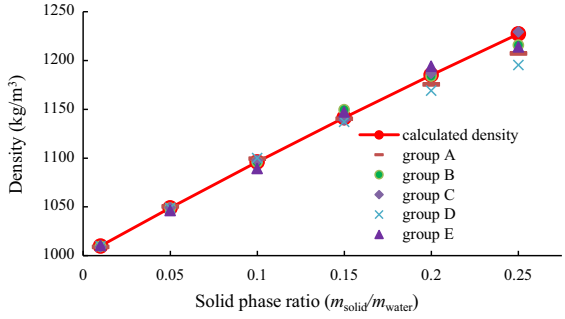

Fig. 5 Measured density and theoretical density of each test condition

With help from the video analysis software, the video of each test group condition was analyzed, and the flow velocity changes of clear water and water-stone flow under various test conditions were measured, as shown in Fig. 6. Through comparison, it was found that under the various test conditions, the change in the water-stone flow velocity of each working group and working conditions was very small (probably because the solid phase occupied a

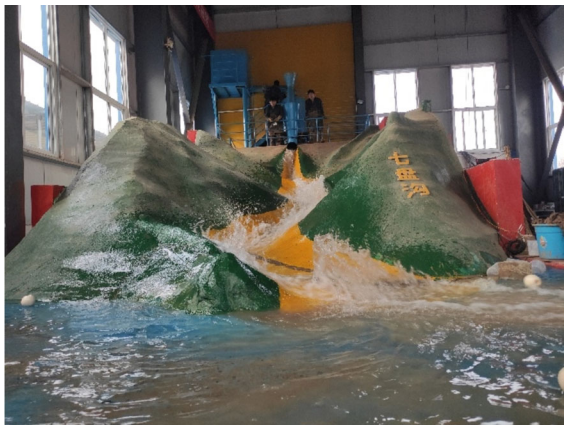

Fig. 6 Measurement of flow velocity of water flow and water-stone flow under various conditions

relatively small proportion in the test and had only a minor effect on the water flow velocity). Therefore, the water-stone flow velocity could be uniformly expressed by the clear water flow velocity, and consequently the change in the water-stone flow velocity with time observed was as shown in Fig. 7.

3.2 Basic processing of impact acceleration signal data

As per the set test conditions, the gravel sized crushed stone particles were configured and the tests were carried out. The dynamic signal test system collected information for the impact acceleration time history curve of the 31 sets of test conditions. As a typical example, the original impact acceleration time history curve for C4 condition was as shown in Fig. 8. This curve clearly indicates the instant when the supporting structure was impacted by the water flow as the vibration acceleration of the supporting structure instantly increased. With decrease in the flow, velocity

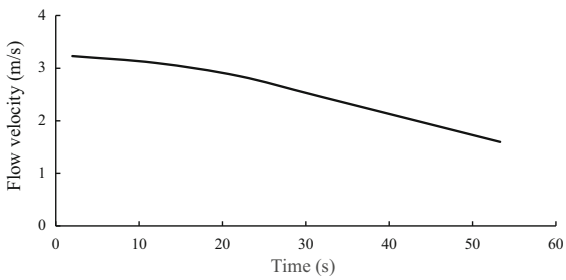

Fig. 7 Time-history curve of flow velocity

of the water-stone flow and the damping action of the supporting structure, the impact acceleration showed a non-linear decrease and then gradually stabilized.

The tail end of the collected impact acceleration signal data stabilized eventually to a long signal apparently useless as it is void of any information. The original signal was "pinching and unwinding" and the time was unified for further analysis (Fig. 8, the original signal is shown in the inset at the upper right corner of the figure).

3.3 Autocorrelation analysis of impact acceleration signal

An autocorrelation of the impact acceleration signal refers to the degree of similarity between a segment of its own signal and each of the other segments of the signal. Throughout the correlation analysis of the signal, the dependence of the amplitude of the impact acceleration signal at two different moments were described, and then the relationship between the signal amplitude and the fluid velocity was reflected.

The autocorrelation function reflected the degree of correlation between the values at different times over the same sequence. Periodic signal corresponding to a period of T was $x(t)$. The autocorrelation function $R_x(\tau)$ and the correlation coefficient $\rho_x(\tau)$ were defined as (Wang et al. 2019; Yang et al. 2014):

$$R_x(\tau) = \lim_{T\to\infty} \frac{1}{T} \int_0^T x(t)x(t+\tau)d_t \tag{2}$$

$$\rho_x(\tau) = \frac{R_x(\tau) - \mu_x^2}{\sigma_x^2} \tag{3}$$

where t is impact time (s); τ is the delay of impact acceleration signal; μ_x is the mean value of the signal; σ_x is the standard deviation of the signal.

The above formula was programmed in MATLAB, and the correlation analysis of impact acceleration signal was carried out with C4 condition as an example. The signal in Fig. 8 is a segment taken from the complete impact signal. The autocorrelation of complete signal and two intercepted signals were analyzed to judge the stability of shock response, the analysis results are shown in Fig. 9. The figure (a) is the autocorrelation of the complete impact signal under C4 condition, and the figure (b) and (c) represent autocorrelation of the two intercepted signals.

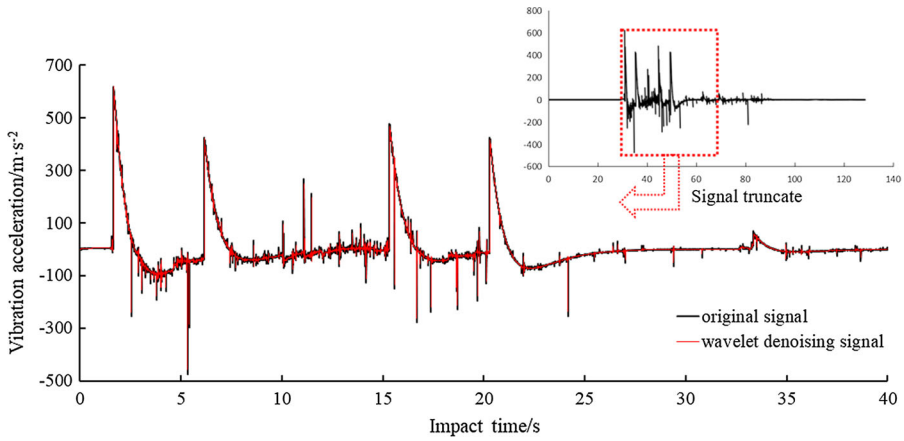

Fig. 8 Whole and part time-history curve of impact acceleration under test condition C4

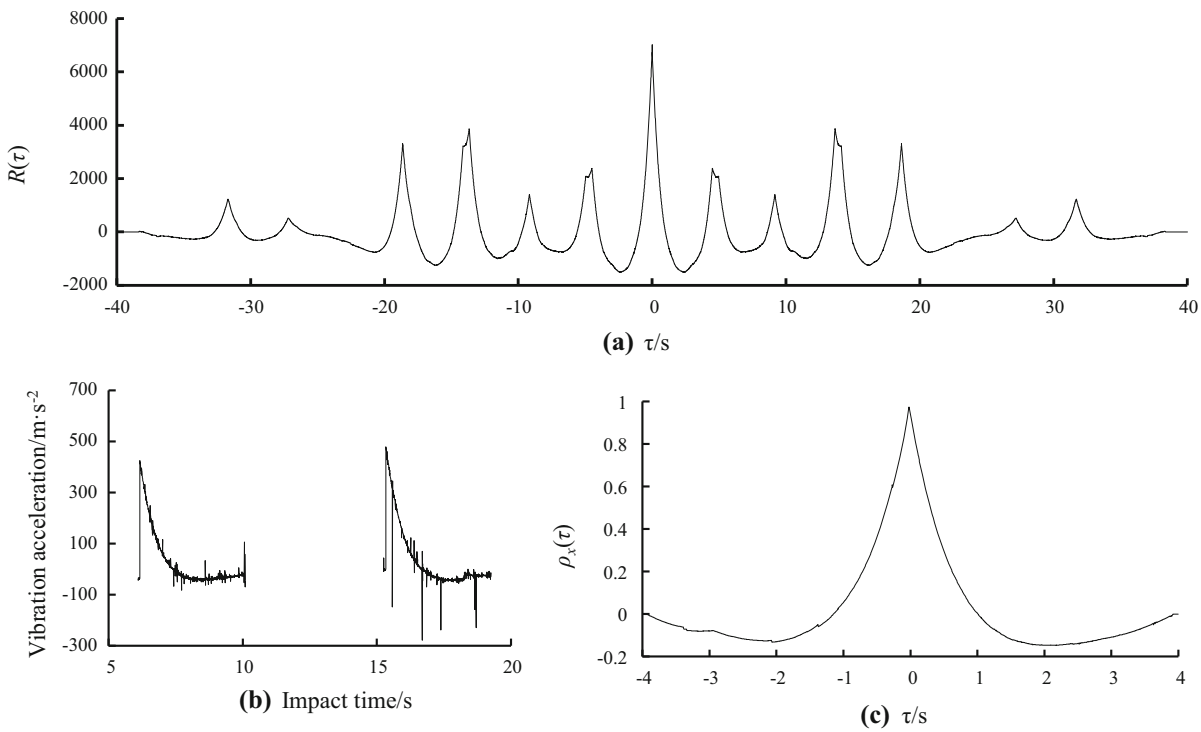

Fig. 9 Autocorrelation coefficient of τ test condition C4

The results show that the autocorrelation curve of the complete signal of C4 condition shows a peak value of 7010.39 when $\tau = 0$, and the two sides are aperiodic fluctuation. The autocorrelation curves of similar shape can also be obtained by analyzing other conditions. It shows that the impact of water-stone flow vibrates obviously, but the periodicity is poor.

From the figure (b) and figure (c) in Fig. 9, it can be seen that the correlation coefficient of the two intercepted signals reaches 0.9748, indicating that they are highly correlated. It shows that the impact acceleration signal of water-stone flow is very stable under the same condition.

4 Impact acceleration signal spectrum and energy analysis

4.1 Frequency spectrum analysis of impact acceleration signal

The impact acceleration signal was usually composed of a real signal and a noise signal. According to previous research results, debris flow impact signals (Tang et al. 2013; He et al. 2016; Chen et al. 2012) and impact acceleration signals (Zhang et al. 2019; Wang et al. 2019) can be processed using wavelet elimination. Accordingly, this research also used the wavelet method (daubechies(db)) to analyze the frequency spectrum distribution and the signal energy distribution characteristics of the impact acceleration signal of water-stone flow.

The db wavelet was used to denoise the signal and extract some hidden features in the acceleration signal. The regularity of the extracted, detailed information increased with increase of the decomposition layer. In order to satisfy the extraction of the detailed information of the acceleration signal, this paper used the db wavelet to decompose the impact acceleration signal of the water-stone flow with 8-layer wavelet.

The above method was programmed into MATLAB software to realize the Fast Fourier Transformation (FFT), decomposition and reconstruction of the shock acceleration signal. Taking the impact acceleration signal of C4 working condition as an example, the decomposed and reconstructed frequency spectrum signal of each frequency band is shown in Fig. 10. The statistical analysis characteristics of the spectrogram are shown in Table 2. After decomposition, 8 frequency band signals (Eq. 4), the signal peak value and the frequency distribution of each band were obtained (Table 2).

$$f(t) = a_8 + d_8 + d_7 + d_6 + d_5 + d_4 + d_3 + d_2 + d_1 \tag{4}$$

where a_8 is the approximate coefficient; d_1–d_8 is the detailed coefficients of each decomposition layer.

From the water-stone flow in Table 2 (the decomposed spectrum of C4 working condition, as was shown in Fig. 10) and the spectrum analysis of the impact acceleration signal of clear water working condition, it was inferred that the impact acceleration signal was steep and single-peaked in the low frequency range, but gradually converted to a flat single peak in the high frequency range.

4.2 Energy distribution characteristics of impact acceleration signal

There are two main methods for describing signals in the frequency domain: energy spectrum and power spectrum. The power spectrum was for periodic signals, and the energy spectrum was for time-limited non-periodic signals. The impact of water-stone flow was a non-periodic signal, which was therefore analyzed using energy spectrum. The frequency spectrum analyses of the signal gave the energy distribution at each frequency, and then obtain the frequency value of the main amplitude and energy distribution. Based on the wavelet transform method, the water-stone flow impact acceleration signal was transformed by FFT to obtain the change law of the impact acceleration signal in different frequency bands. The energy distribution of the impact acceleration signal was obtained using the following integral calculation.

$$\begin{aligned} E &= \int_{-\infty}^{+\infty} x^2(t)dt \\ &= \sum_{i=1}^{N} \int_{-\infty}^{+\infty} f_i^2(t)dt + \sum_{m\neq n} \int_{-\infty}^{+\infty} \omega_m(t)\omega_n(t)dt \end{aligned} \tag{5}$$

where $x(t)$ is the original signal; $f_i(t)$ is the ith (i = 1, 2, …, N) low-frequency signal obtained after wavelet decomposition, and N is the total number of low-frequency signals after decomposition; $\omega_m(t)$ and $\omega_n(t)$ are the high-frequency signals obtained after wavelet decomposition.

As a consequence of the orthogonal characteristics of the wavelet, the j (j = 1, 2, …, N + K) frequency band signal $\omega_j(t)$ obtained after wavelet decomposition was simplified to $x(t)$, and the total energy was simplified to:

$$E = \sum_{j=1}^{N+K} \int_{-\infty}^{+\infty} \omega_j^2(t)dt = \sum_{j=1}^{N+K} E_j \tag{6}$$

$$E_j = \int_{-\infty}^{+\infty} \omega_j^2(t)dt \tag{7}$$

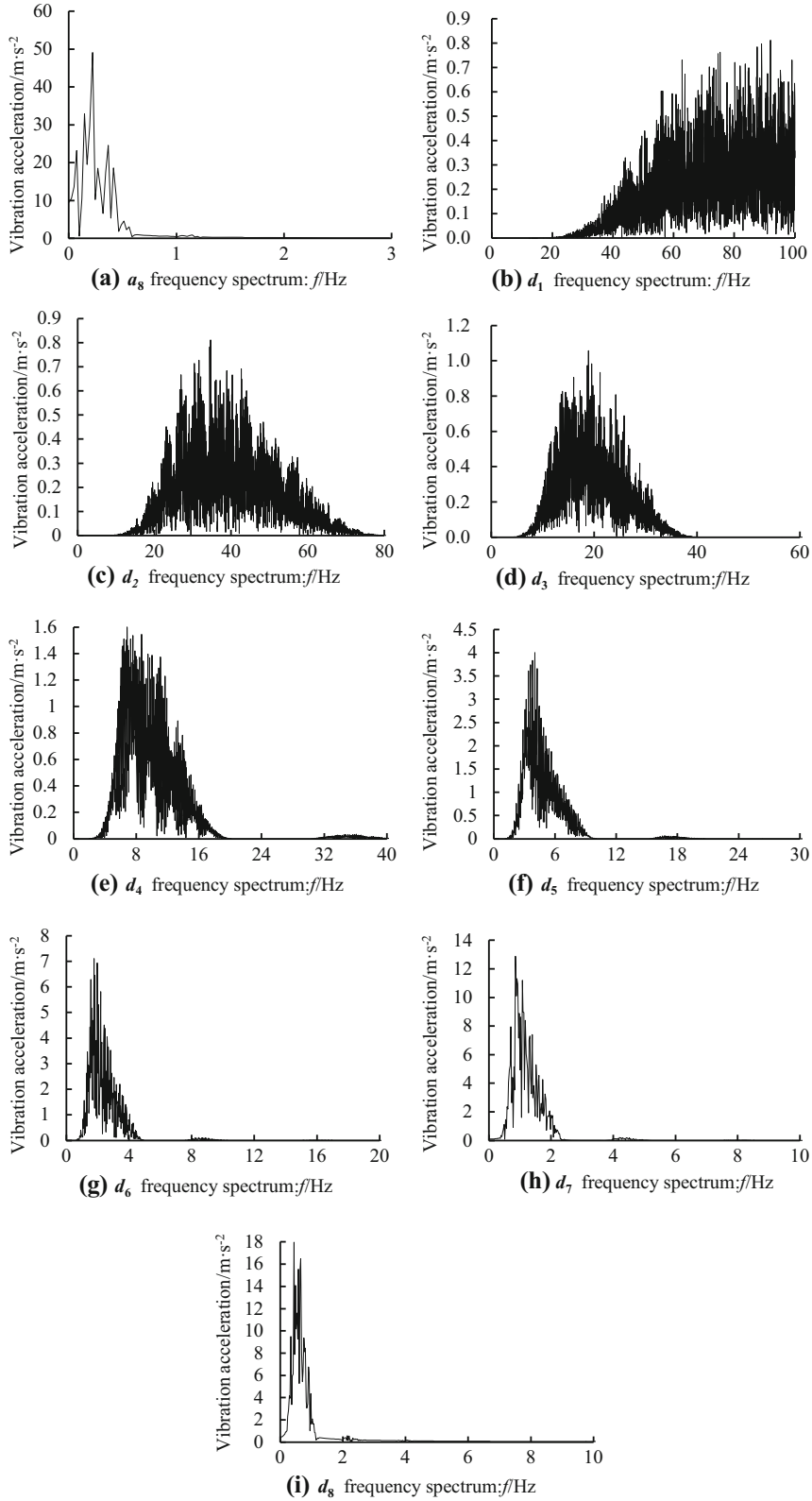

Fig. 10 Analytical spectrum of impact acceleration under test condition C4

Table 2 Statistical table of shock signal spectrum characteristics

Serial number	Frequency spectrum (Hz)	Signal peak of C4 (m s^{-2})	Signal peak of q (m s^{-2})
Approximation coefficient: a_8	0–0.3905	49.061	0.586
Detail coefficients: d_8	0.3905–0.781	17.976	0.022
Detail coefficients: d_7	0.781–1.562	12.878	0.019
Detail coefficients: d_6	1.562–3.125	7.108	0.011
Detail coefficients: d_5	3.125–6.25	4.003	0.001
Detail coefficients: d_4	6.25–12.5	1.600	0.001
Detail coefficients: d_3	12.5–25	1.057	0.001
Detail coefficients: d_2	25–50	0.812	0.002
Detail coefficients: d_1	50–100	0.811	0.004

$$E_j/E = \int_{-\infty}^{+\infty} \omega_j^2(\mathrm{t})dt / \sum_{j=1}^{N+K} \int_{-\infty}^{+\infty} \omega_j^2(t)dt \tag{8}$$

where E_j is the ability of the jth high-frequency signal.

Based on this and through MATLAB programming, the impact acceleration signals from the 31 groups of working conditions were subjected to wavelet transformation to obtain the corresponding wavelet transformation reconstruction signal, frequency spectrum, frequency band and other information. Taking the C4 working condition as an example, the reconstructed impact acceleration signal after wavelet transformation was as shown by the red line in Fig. 10. Further calculations gave the energy distribution of the signal. The impact acceleration signals of the 31 groups of working conditions were imported into the MATLAB program to calculate the energy analysis of the respective signals. The percentage of energy in each frequency band (a_8–d_8) to the total energy of the signal was as shown in Fig. 11. The ordinate in Fig. 11 is the energy percentage of the impact acceleration signal, and the abscissa is the natural logarithm of the maximum frequency in each frequency band (for example, the frequency of the a_8 frequency band is 0–0.3905 Hz, and the natural logarithm of 0.3905 was taken as the abscissa).

It was evident from the analysis in Fig. 11 that the energy of the impact acceleration signal of the clear water flow and the water-stone flow were mainly concentrated in the low frequency band (a_8). Compared with the clear water flow, the energy distribution of the impact acceleration signal of the water-stone flow was more extensive. This could be distributed to the low-frequency frequency range from d_8 to d_5, and the mid-high frequency range from d_4 to d_1 was dominated by noise signals. The general trend of the energy distribution of the impact acceleration signal of water-stone flow gradually decreased with increasing frequency, but due to the pulsating characteristics of water-stone flow, the decreasing trend of each working condition was not consistent (Fig. 12), such as the trend of signal energy reduction fluctuated at the frequency bands a_8 and d_8 in the A4 working condition. At the same time, the impact signal energy of water-stone flow increased with the increase of solid-to-liquid ratio and particle size. Under the same solid-to-liquid ratio condition, the energy of the impact signal was approximately positively correlated with the solid particles. The larger the solid-to-liquid was, the more obvious the energy increase of the impact signal was.

Further analysis of Fig. 11 showed that there was an obvious exponential relationship between the upper and lower limits of the impact acceleration signal energy percentage of the water-stone flow and the frequency. By adopting the asymptotic fitting of the data, the correlation coefficient of the fitting relation (R^2) was around 0.994. It confirmed that under test conditions, the energy ratio of the impact signal from the water-stone flow was distributed within the envelope range of the fitting relationship. In actual engineering, the impact of low frequency bands should be mainly prevented from acting on the engineering structures designed to mitigate flood disasters, and this frequency range was 0–0.4 Hz. For water-stone flow

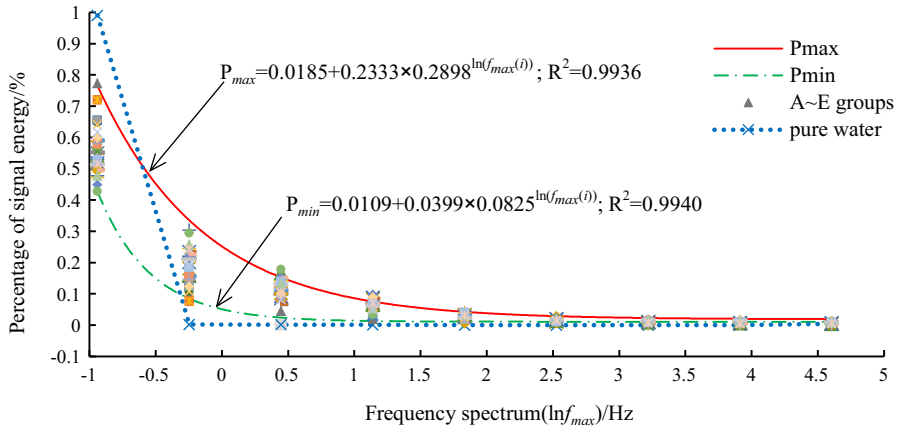

Fig. 11 Energy percentage of impact acceleration signal under test conditions

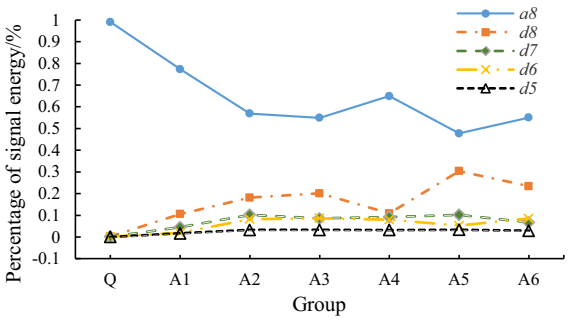

Fig. 12 Energy distribution of impact acceleration under test condition Q and A

disasters, the impact of low frequency band should be considered, and the frequency range was 0–6.25 Hz.

5 Conclusions

Through the analysis of both test data and image data from testing the 31 groups of working conditions, the following main conclusions were obtained:

(1) The autocorrelation curve of the shock acceleration signal had a peak value when $\tau = 0$, and there were non-periodic fluctuations on both sides, indicating that the vibratory movement of water and rock flow was obvious despite the periodicity being poor. Two adjacent segments of pulse signals in the same signal were highly correlated, and the impact acceleration signal generated by water and rock flow was highly stable. The test provided a new methodology for studying the impact characteristics from debris flow.

(2) The wavelet theory was used to transform and extract information from the impact acceleration signal of water-stone flow. The maximum value of the impact acceleration signal of water-stone flow was located in the low frequency at the approximate coefficient a_8 frequency band. The maximum amplitude of each frequency band was attenuated from low frequency (a_8: 0–0.3905 Hz) to high frequency (d_5: 3.125–6.25 Hz), but the attenuation amplitude gradually decreased. It means the effective signal of water-stone flow impact was between 0 and 6.25 Hz, and the remaining mid-high frequency bands are mainly noise signals. The water-stone flow protection structure should mainly consider the impact of the middle and low frequency bands (0–6.25 Hz).

(3) The energy of the impact acceleration signal of clear water flow and water-stone flow were mainly concentrated in the low frequency band (a_8), accounting for 99.1% and 42.7–77.3% respectively. The energy distribution of the impact acceleration signal of water-stone flow generally decreased with the increasing frequency, but it was volatile. There was evidence of asymptotic exponential relationship between the upper and lower limits of the energy percentage from the impact acceleration signal and the natural logarithm of the frequency, and the correlation coefficient was more than 0.990.

Acknowledgements This research was supported by the National Program on Key Research Project of China (Grant No. 2018YFC1505405).

Data availability The acquisition of experimental data is obtained by the physical model experiment conducted in a debris flow simulation laboratory at Zaozhuang University (Shandong, China). The experimental results are repeatable. Relevant scholars can use similar experimental models or visit the laboratory to further verify the reliability of the experimental data.

Declaration

Conflict of interest The authors declare that they have no conflict of interest.

References

Chechelnitsky VV, Makarov SA, Dobrynina AA (2018) The Disastrous water-stone flow in the Kyngarga River (Republic of Buryatia) on June 27–29, 2014, according to Seismological Data. Doklady Earth Sci 481(PT.2):1108–1112

Chen HK, Xian XF, Tang HM, Zhang YP, He XY, Wen GJ, Tang L (2012) Energy distribution in spectrum of shock signal for non-viscous debris flow. J Vib Shock 31(14):56–59

Chen XH, Sun HY, Mei C, Zhang WJ, Qian WJ (2016) Flow control of water-stone flow star. Mountain Res 34(2):194–199

Cui P (2009) Advances in debris flow prevention in China. Sci Soil Water Conserv 7(5):7–13

Ding P, Tao LJ, Yang XR, Zhao J, Shi C (2019) Three-dimensional dynamic response analysis of a single-ring structure in a prefabricated subway station. Sustain Cities Soc 45:271–286

Guo S, Xu P, Zheng Z, Gao Y (2014) Estimation of flow velocity for a debris flow via the two-phase fluid model. Nonlinear Process Geophys Discuss 1:999–1021

He XY, Tang HM, Chen HK (2014) Experimental study on impacting characteristic of debris flow considering different slurry viscosities, solid phase ratios and grain diameters. Chin J Geotech Eng 36(5):977–982

He XY, Chen HK, Tang HM (2016) Experimental study on the energy distribution characteristics of impacting signals of debris flow considering the slurry viscosity and particle collision. J Vib Shock 35(6):64–69

Hu KH, Wei FQ, Li Y (2011) Real-time measurement and preliminary analysis of debris-flow impact force at Jiangjia Ravine, China. Earth Surf Proc Land 36:1268–1278

Ma QH, Yin HX, Liu YF, Niu BB (2016) Model study on catastrophe characteristics for initiation debris-flows in Taihang Mountain Area. Yellow River 38(11):5–8

Nearing MA, Simanton JR, Darrell NL, Bulygin SJ (1999) Soil erosion by surface water flow on a stony, semiarid hillslope. Earth Surf Proc Land 24(8):677–686

Savage SB (1979) Gravity flow of cohesionless granular materials in chutes and channels. J Fluid Mech 92(1):53–96

Strutinskiy V, Yakhno O, Machuga O, Hnativ I, Hnativ R (2018) Analysis of interaction between a configurable stone and a water flow. East-Eur J Enterp Technol 6(96):14–20

Tang JB, Hu KH, Zhou GD, Chen HY, Zhu XH, Ma C (2013) Debris flow impact pressure signal processing by the wavelet analysis. J Sichuan Univ (eng Sci Ed) 45(1):8–13

Wang LF, Zhu HZ, Song NN, Zou Z, Yao CY (2019) Impact signal dynamic characteristics of energy dissipation shed tunnel. J Traffic Transp Eng 19(5):33–41

Wang H, Chen HK, Zhang JH, Wang Q (2020) Experimental study on influence of impact angle of Mounta torrent on distribution rule of impact force on subgrade. J Chongqing Jiaotong Univ (nat Sci) 39(5):97–102

Wu WL, Liu XL, Guo JQ, Sun FY, Huang X, Zhu ZG (2021) Upper limit analysis of stability of the water-resistant rock mass of a karst tunnel face considering the seepage force. Bull Eng Geol Environ 80:5813–5830

Xu YN, Liang ZY, Su XB, Wang L (2000) Physical modeling of debris flow in the experiment flume. J Nat Disasters 9(4):105–110

Yang M, Ma DT, Chen Y (2014) An approach about water stone flow hazards occurred in July 18th, 2013 in Maoniuping rare earth mining area in Mianning. Sichuan Mt Res 32(6):732–738

Yang Q, Ma H, Ji XR (2014) Parameter extraction of traffic noise by analysis of auto-correlation function and inter-aural cross-correlation function. Acta Acust 39(5):624–632

Zhang YP (2009) Signal identification method to debris flow impaction. Master's thesis, Chongqing Jiaotong University, Chongqing

Zhang Y, Li GW, Yang JH, Guo XF (2019) Application of improved wavelet threshold function in impact acceleration signal processing. Chin J Sens Actuators 32(3):405–410

Zhuang HY, Hu ZH, Wang XH, Chen GX (2015) Seismic responses of a large underground structure in liquefied soils by FEM numerical modelling. Bull Earthq Eng 13:3645–3668